Hindawi Publishing Corporation
Shock and Vibration
Volume 2016, Article ID 1067506, 8 pages
http://dx.doi.org/10.1155/2016/1067506

Research Article

Active Magnetic Bearings Stiffness and Damping Identification from Frequency Characteristics of Control System

Chaowu Jin, Yuanping Xu, Jin Zhou, and Changli Cheng

College of Mechanical and Electrical Engineering, Nanjing University of Aeronautics and Astronautics, Nanjing 210016, China

Correspondence should be addressed to Jin Zhou; zhj@nuaa.edu.cn

Received 28 July 2015; Accepted 18 October 2015

Academic Editor: Jörg Wallaschek

At present, the stiffness and damping identification for active magnetic bearings (AMBs) are still in the stage of theoretical analysis. The theoretical analysis indicates that if the mechanical structure and system parameters are determined, AMBs stiffness and damping are only related to frequency characteristic of control system, ignoring operating condition. More importantly, few verification methods are proposed. Considering the shortcomings of the theoretical identification, this paper obtains these coefficients from the experiment by using the magnetic bearing as a sine exciter. The identification results show that AMBs stiffness and damping have a great relationship with the control system and rotating speed. Specifically, at low rotating speed, the stiffness and damping can be obtained from the rotor static suspension by adding the same excitation frequency. However, at high speed, different from the static suspension situation, the AMBs supporting coefficients are not only related to the frequency characteristics of control system, but also related to the system operating conditions.

1. Introduction

From the dynamic point, the AMBs rotor system can operate stably since the AMBs can provide appropriate supporting stiffness and damping parameters (bearing parameters) for the rotor. Now, the researches on AMB supporting parameters identification are mainly from two aspects.

One idea is from the mechanical bearing parameters identification. Through the relationship between the excitation and rotor bearing system response, the bearing parameters can be identified through the identification algorithm along with experiment. Based on the unbalance response of rotor bearing system, Zhou and Ni [1] identified the AMBs stiffness and damping of rigid rotor bearing model and verified identification by finite element simulation. Zhang et al. [2] set the modal parameters of AMBs rotor system as the target response, using the complex modal model updating technology, and identified AMBs stiffness and damping under static suspension. De Santiago and San Andrés [3, 4] identified these coefficients for mechanical bearing from transient rotor dynamic response due to impacts and imbalances. Bi et al. [5] proposed a time-frequency-domain hybrid method of identifying the dynamic characteristic parameters of journal bearings and the unbalance of the rotor on field condition and without artificial excitations. Wang and Xia [6] gave a method and data processing program for extracting the stiffness para meters of the rolling element bearings from random vibration responses. Chen et al. [7] identified the dynamic stiffness and damping of bearing by the boundary element method. Tiwari [8, 9] proposed identification algorithms for the estimation of mechanical bearing parameters and residual unbalances through forced responses of the system. Tiwari and Chakravarthy [10] developed an identification algorithm for the simultaneous identification of the bearing and unbalance parameters for flexible rotor bearing systems by using run-down measurements. The disadvantage of these identification methods for mechanical bearing is that they need to apply excitation to the rotor and an accurate rotor model is indispensable. Test data must be under the rotating situation, which also puts forward higher requirements on excitation forms, system response, and stability of the system.

Identifying the stiffness and damping from the theoretical analysis of AMB control system by obtaining the system transfer function is another identification idea. The AMBs system uses active control strategy; therefore, the supporting parameters are closely related to the system structure and

control strategy. Wang [11] studied the effects of AMB control system frequency response characteristics and structural parameters on the AMBs stiffness and damping and obtains the frequency characteristics of the equivalent stiffness and damping. Zhao et al. [12] studied the AMB rotor system with analog PID controller based on the independent control principle; it showed that the AMBs stiffness and damping were influenced by the differential and proportional coefficient in controller. Humphris et al. [13] obtain the stiffness and damping values for a magnetic bearing at static situation and found that these coefficients of AMBs are affected by the position and velocity feedback parameters of controller. By analyzing the frequency dependent feedback controller transfer function, Williams et al. [14] obtained the equivalent stiffness and damping coefficients theoretically. Under the shaker excitation, Lim et al. [15] experimentally identified a five-degree-of-freedom hybrid magnetic bearing for blood bump applications at static suspension situation with proportional-integral-derivative (PID) controllers. Tsai et al. [16] applied the wavelet transform algorithm to identify the magnetic damping and stiffness coefficients. This identification method had to simplify the control system in order to get the transfer function. But, for some system using the complex control strategy such as adaptive control method, it was very difficult to get the transfer function accurately.

Aiming at the shortages of the researches on AMBs stiffness and damping, this paper uses magnetic bearing as the exciter, tests the frequency characteristics of the control system, obtains the relationship between bearing parameters and frequency characteristics of the control system, and verifies the identified stiffness and damping values. The results show that, at low speed, the bearing parameters of AMBs are mainly related to the controller frequency characteristics, but at high speed, the bearing parameters are not only related to the controller frequency characteristics, but also related to the speed.

The remainder of the paper is organized as follows. Section 2 describes the theoretical basis of the relationship between bearing parameters and frequency characteristics of the control system. The test results of the frequency characteristics of the control system are presented in Section 3 using magnetic bearing as the exciter. Section 4 shows experimental verification in order to validate the proposed method. Conclusions are drawn in Section 5.

2. Fundamental

The structure of radial AMB with single degree of freedom used in this paper is shown in Figure 1. Table 1 shows its specific parameters.

The electromagnetic force generated by a pair of differential magnetic poles in the figure can be expressed as

$$F(t) = \frac{\mu_0 A N^2}{4} \cos\beta \left[\frac{(I_0 - i(t))^2}{(x_0 - x(t))^2} - \frac{(I_0 + i(t))^2}{(x_0 + x(t))^2} \right]. \quad (1)$$

As shown in (1), the electromagnetic force of differential arrangement AMB is nonlinear related to the displacement $x(t)$ and the control current $i(t)$. The nonlinearity of the electromagnetic force is detrimental for the application of linear

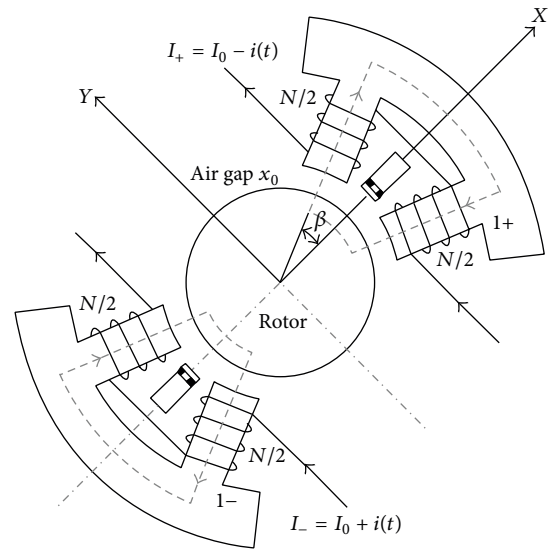

Figure 1: The structure principle diagram of radial AMB with single degree of freedom.

Table 1: The related parameters of radial AMB.

Parameter	Value
Coil number of signal-pole N	120
Magnetic pole area A/m^2	2×10^{-4}
Bias current I_0/A	1
Air gap x_0/mm	0.3
Permeability of vacuum μ_0	$4\pi \times 10^{-7}$
Pole angle β/°	22.5

control theory, so linear analysis of the formula is necessary, which can be expressed as

$$F(t) = -k_{x0} \cdot x(t) + k_{i0} \cdot i(t), \quad (2)$$

where k_{x0}, k_{i0} are displacement stiffness and current stiffness of radial AMBs at the equilibrium position, respectively, which can be written as follows:

$$k_{x0} = \frac{\mu_0 A N^2 I_0^2 \cos\beta}{x_0^3}, \qquad k_{i0} = -\frac{\mu_0 A N^2 I_0 \cos\beta}{x_0^2}. \quad (3)$$

Because of the complete symmetry of the AMB radial structure, one degree of freedom of the radial AMB system can be the research object; control block diagram of a one degree-of-freedom system is shown in Figure 2.

I_0 and $i(t)$ are the bias current and the control current into the electromagnet coil, respectively; v_s is the voltage signal converted from the rotor displacement by the displacement sensor, which has a linear relationship with the rotor vibration displacement $x(t)$; v_c is the input of controller; c_r is the gap between the catcher bearing and rotor, named protective gap, which is usually half of air gap x_0; v_0 is reference voltage

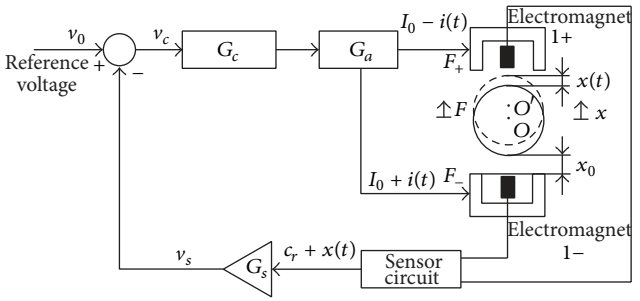

Figure 2: Control block diagram of one degree-of-freedom radial AMB system.

of controller, which is to multiply displacement gain by protective gap; G_a, G_s, and G_c are the transfer function of the power amplifier, the displacement sensor, and the PID controller, respectively.

According to the block diagram of control system, the relationship between control current and rotor vibration displacement is obtained:

$$\begin{aligned} i(t) &= v_c \cdot G_c \cdot G_a = (v_0 - v_s) \cdot G_c \cdot G_a \\ &= [v_0 - (c_r + x(t)) \cdot G_s] \cdot G_c \cdot G_a \\ &= -x(t) \cdot G_s \cdot G_c \cdot G_a \quad v_0 = c_r \cdot G_s. \end{aligned} \tag{4}$$

Take (4) into (2):

$$F(t) = -k_{x0} \cdot x(t) - k_{i0} \cdot G_s \cdot G_c \cdot G_a \cdot x(t). \tag{5}$$

Laplace transform (5):

$$F(s) = [-k_{x0} - k_{i0} \cdot G_s(s) \cdot G_c(s) \cdot G_a(s)] \cdot x(s). \tag{6}$$

AMBs generalized stiffness is the ratio of electromagnetic force Laplace transformation and rotor displacement Laplace transformation; that is,

$$K(s) = \frac{F(s)}{x(s)} = -k_{x0} - k_{i0} \cdot G_s(s) \cdot G_c(s) \cdot G_a(s). \tag{7}$$

One degree-of-freedom bearing force with the spring damping characteristics can be expressed as

$$f(t) = k \cdot x(t) + c \cdot \dot{x}(t). \tag{8}$$

Transform (8) by Laplace transform and get the generalized stiffness:

$$K'(s) = \frac{f(s)}{x(s)} = k + c \cdot s. \tag{9}$$

Considering the frequency characteristics of the generalized stiffness, take $s = j\omega$, so (7) and (9) are

$$\begin{aligned} K(j\omega) &= -k_{x0} - k_{i0} \cdot G_s(j\omega) \cdot G_c(j\omega) \cdot G_a(j\omega), \\ K'(j\omega) &= k + c \cdot j\omega. \end{aligned} \tag{10}$$

From (10), the magnetic bearing equivalent stiffness and damping can be written as

$$\begin{aligned} k &= -k_{x0} - k_{i0} \cdot \mathrm{Re}[G_s(j\omega) \cdot G_c(j\omega) \cdot G_a(j\omega)], \\ c &= -\frac{k_{i0} \cdot \mathrm{Im}[G_s(j\omega) \cdot G_c(j\omega) \cdot G_a(j\omega)]}{\omega}, \end{aligned} \tag{11}$$

where $\mathrm{Re}[G_s(j\omega) \cdot G_c(j\omega) \cdot G_a(j\omega)]$ and $\mathrm{Im}[G_s(j\omega) \cdot G_c(j\omega) \cdot G_a(j\omega)]$ in the equation represent the real and imaginary parts of $G_s(j\omega) \cdot G_c(j\omega) \cdot G_a(j\omega)$, respectively, where ω is the external excitation frequency, rather than the speed of rotor. Seen by (11) in certain control parameters, and ignoring the influence of eddying effect, the equivalent stiffness and damping of the radial AMB are only related to the external excitation frequency ω, which has nothing to do with the rotor speed Ω unless the excitation is due to unbalance rotor, in which the excitation frequency and rotor speed are clearly related.

By formula transformation, (4) can be expressed as

$$G_s(j\omega) \cdot G_c(j\omega) \cdot G_a(j\omega) = -\frac{i(j\omega)}{x(j\omega)} = -\frac{i_A}{x_A} e^{(\varphi_i - \varphi_x)}, \tag{12}$$

where x_A and i_A are the amplitude of the rotor displacement and control current, respectively, and φ_x and φ_i are the phase of displacement and control current, respectively. If the amplitude and phase of control current $i(t)$ and rotor displacement $x(t)$ can be obtained by testing method, the frequency characteristics of $G_s(j\omega) \cdot G_c(j\omega) \cdot G_a(j\omega)$ and AMBs equivalent stiffness and damping can also be obtained. According to the characteristics of AMB system, it can test the frequency characteristics of the control system loop using AMB as an incentive. Schematic of the excitation applied way is shown in Figure 3.

Using signal generator to generate a signal with frequency ω and amplitude 1 V, put this signal to the input of the power amplifier 1 corresponding to the 1+ magnetic pole. At this time, the coil current of 1+ magnetic pole includes bias current I_0, feedback control current $i(t)$, and external excitation current $i_e(t)$. The rotor displacement signal $x(t)$ and the control current $i(t)$ of 1− pole coil will be collected, respectively. The data will be substituted into (6) to get the amplitude ratio and phase difference. Change the excitation frequency and repeat the testing process, the frequency characteristic curve of $G_s(j\omega) \cdot G_c(j\omega) \cdot G_a(j\omega)$ about ω can be drawn, and the equivalent stiffness and damping of AMBs can be obtained with the combination of (11).

3. Experimental Investigations

According to the structural parameters in Table 1, displacement stiffness k_x and current stiffness k_i at different rotor displacement x and control current i can be obtained by using the finite element analysis method, as shown in Figure 4.

Current stiffness k_{i0} and displacement stiffness k_{x0} of the rotor at the equilibrium position can be obtained by taking the structure parameters of Table 1 into (3). The value at $x = 0$ and $i = 0$ in Figure 4 is the current stiffness k_{i0}

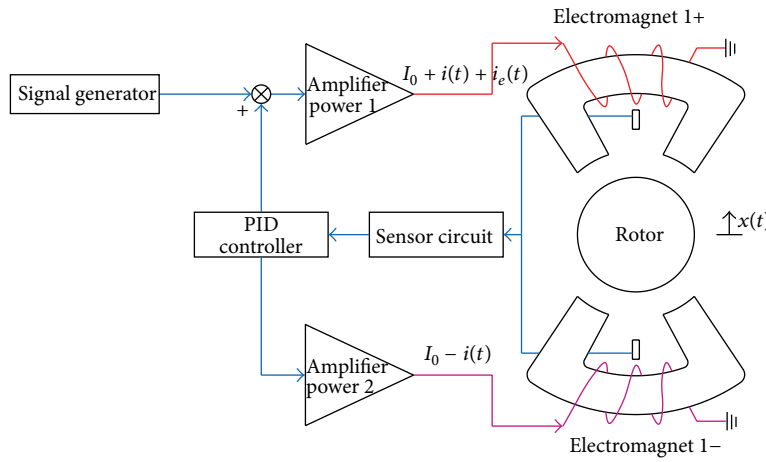

Figure 3: Schematic of the excitation applied way.

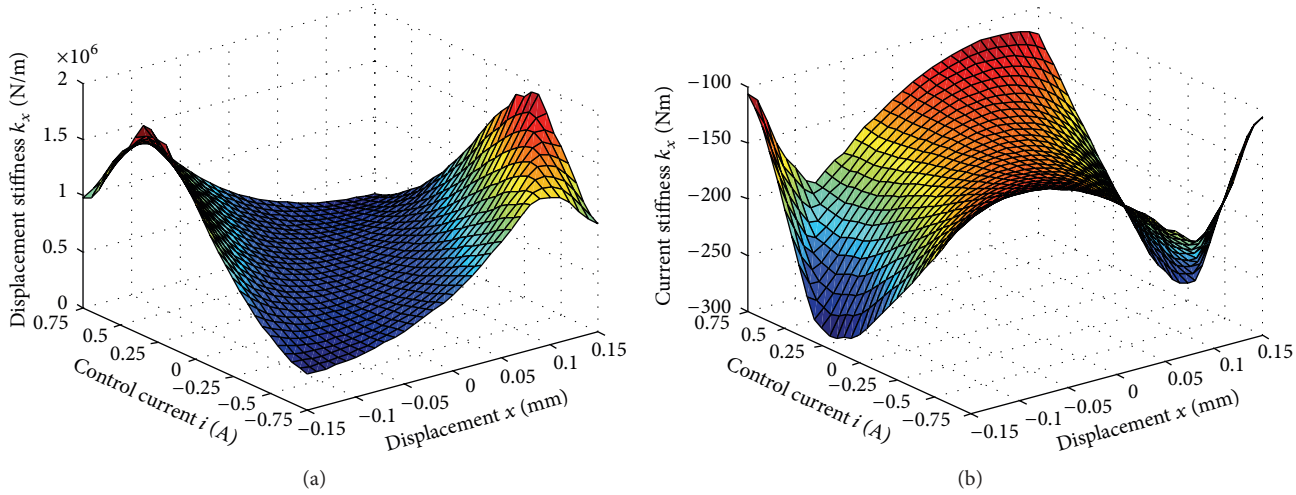

Figure 4: Current stiffness (a) and displacement stiffness (b) of finite element analysis.

and displacement stiffness k_{x0} of the rotor at the equilibrium position calculated by finite element method. List k_{x0} and k_{i0} at the equilibrium position in Table 2, which are obtained by finite element method and theoretical calculation.

From Table 2, we can see that values of finite element analysis and theoretical calculation are very close, but the displacement stiffness and current stiffness calculated by finite element method are less than the theoretical calculation values. The reason is that, in the theoretical calculation, the magnetic reluctance, magnetic leakage, magnetic saturation, and other factors of silicon steel sheets are ignored. In order to get accuracy stiffness and damping, we adopt k_{x0} and k_{i0} calculated from finite element analysis in the following.

When the external excitation frequency is less than the cutoff frequency of displacement sensor and power amplifier, it can be seen as a proportional component. In this paper, the transfer function of displacement sensor can be written as $G_s = 2.5/c_r$, the transfer function of power amplifier can be written as $G_a = 2I_0/10$, and the transfer function for PID controller can be written as

Table 2: k_{x0} and k_{i0} at the equilibrium position of radial AMB.

Name	Values of theoretical calculation	Values of finite element analysis
Displacement stiffness k_{x0}/N/m	4.639×10^5	4.507×10^5
Current stiffness k_{i0}/N/A	-1.5063×10^2	-1.4906×10^2

$$G_c = K_p + \frac{K_i}{s} + \frac{K_d s}{1 + \tau_d s}, \tag{13}$$

where K_p, K_i, and K_d are the proportional coefficient, the integral coefficient, and the differential coefficient, respectively, and τ_d is the filtering time constant. The parameters of

Table 3: Parameters of the controller by testing.

Direction	K_p	K_i	K_d	τ_d/s
1#	7.15	32.93	$2.7e-3$	$5.69e-6$
2#	6.85	32.06	$2.6e-3$	$7.79e-6$
3#	8.19	39.69	$3.2e-3$	$6.42e-6$
4#	8.21	39.12	$3.1e-3$	$6.33e-6$

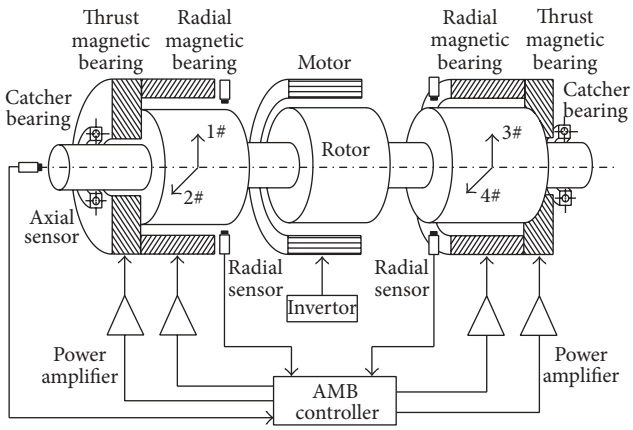

Figure 5: Structure of AMB system.

the controller are shown in Table 3; the frequency characteristic of the controller can be calculated by taking the controller parameters into (13).

Figure 5 shows the studied AMBs system structure, the left radial AMBs are 1# and 2#, and the right radial AMBs are 3# and 4#. The experimental test rig is pictured in Figure 6.

Theoretical values of $G_s(j\omega) \cdot G_c(j\omega) \cdot G_a(j\omega)$ can be obtained by multiplying the transfer function of displacement sensor, power amplifier, and controller and analyzing frequency characteristics. In order to acquire the experimental data, signal generator is employed to drive the external current and NI data acquisition card is employed to record the current and displacement values according to the principle and method of Figure 3. Then use one-order Fourier series based on the least square method to fit the filtered signals to get the amplitude and phase data. The initial frequency is 20 Hz and the stop frequency is 400 Hz, tested once every 5 Hz.

Experimental and theoretical values of the control system frequency characteristics are shown in Figure 7, from which it can be observed that theoretical and experimental values trends of the frequency characteristics in all radial bearings of the control system are in good agreement but not perfectly matched with the change of frequency. This may be due to the error of system model and experiment measurement. However, the error at low frequency is relatively small, and the error increases with the increase of frequency. The reason maybe is that the displacement sensor and power amplifier cannot always be considered as a proportional part in high frequency.

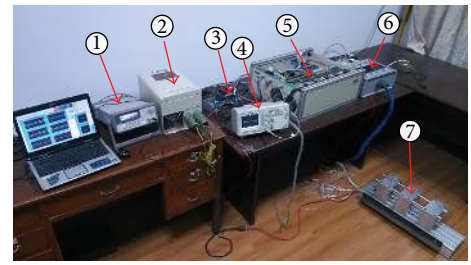

(1) Agilent signal generator
(2) Frequency converter
(3) NI data acquisition card
(4) Agilent oscilloscope
(5) Control box of AMB rotor system
(6) Shunt control box
(7) AMB rotor test rig

Figure 6: AMB unbalance excitation test system.

The equivalent stiffness and damping of each radial AMB can be obtained by substituting testing frequency characteristics of each AMB control system into (11). Figures 8 and 9 are, respectively, the equivalent AMBs stiffness and damping with the change of vibration frequency in 1#, 2#, 3#, and 4#.

According to Figures 7 and 8, in the range of the exciting frequency, the equivalent stiffness and damping in 1# are less than those in 2#; the equivalent stiffness and damping in 3# are less than those in 4#. And with the change of frequency, the equivalent stiffness of each bearing increases, while the equivalent damping of each bearing increases firstly and then decreases slowly, which are broadly consistent with the stiffness and damping of theory analysis in the trend of change.

4. Experimental Verification

Experimental verification is aimed to test the accuracy of the bearing parameter identified in this paper. Equation (11) shows that AMB parameters are only related to the excitation frequency ω, which have nothing to do with the rotor speed Ω when the system structure and control parameters are determined. When the rotor is in unbalanced excitation, the excitation frequency is equal to the rotor speed, $\omega = \Omega$. It means that the stiffness and damping with the rotor speed of Ω are the same as the stiffness and damping coefficient with the rotor in static suspension but the excitation frequency $\omega = \Omega$.

In order to verify the accuracy of the bearing parameters identified in this paper. Firstly, we add unbalance mass on the rotor as the excitation and the rotor unbalance response measurements are conducted for rotor speeds from 20 Hz to 300 Hz. Secondly, the AMB rotor finite element model is built in Patran (a commercial software for Finite Element Analysis). Previous work [17] by us has already detailed the rotor modeling, model updating, and model verification of the updated model. By providing the stiffness and damping values to the bush cell and adding the same unbalance excitation for finite element model, the rotor unbalance response is simulated to obtain the unbalance displacement amplitude.

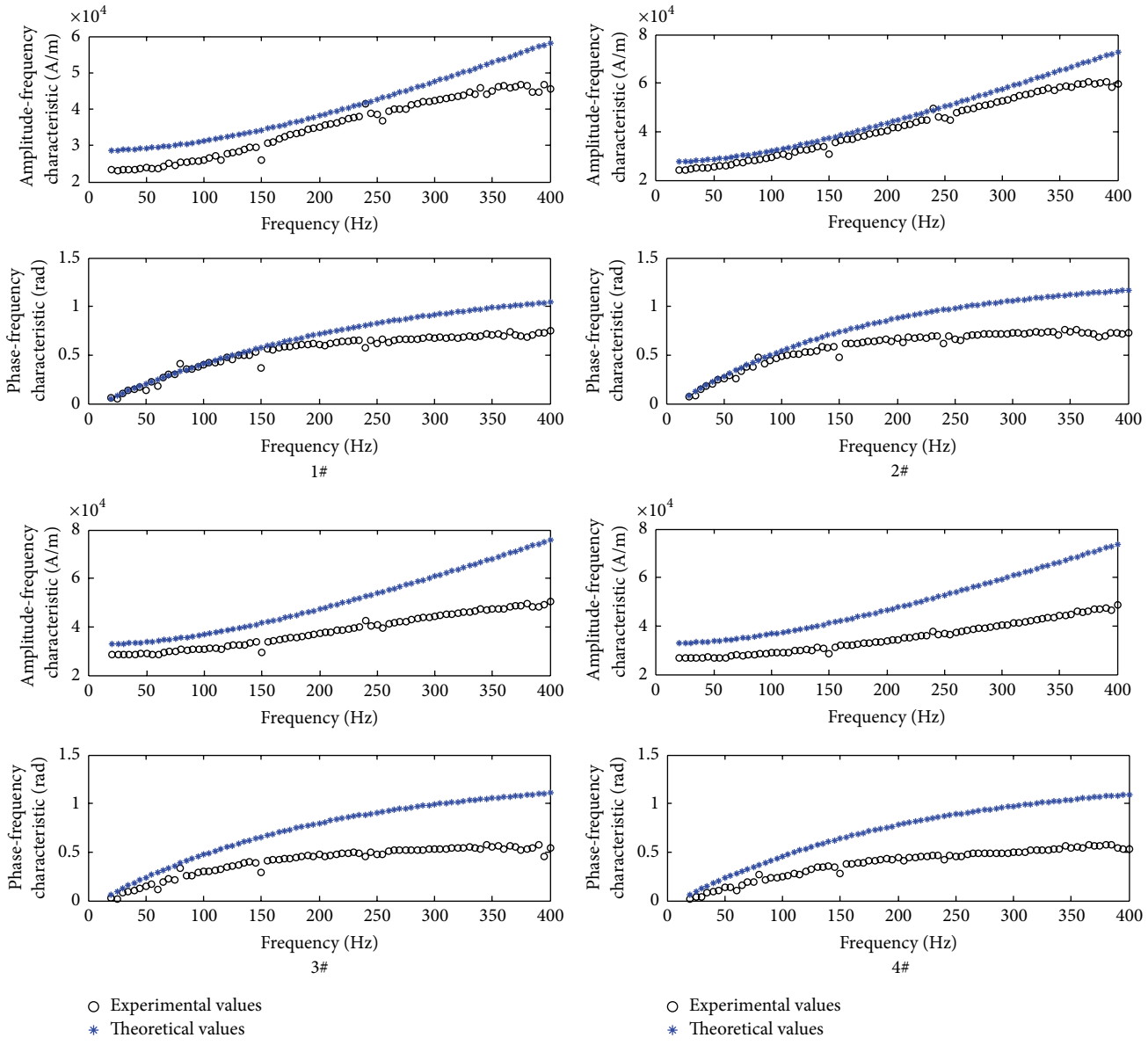

Figure 7: Experimental values and theoretical values of each frequency characteristic.

Finally, we will compare the simulation amplitudes and testing unbalance response amplitudes. Flow chart of verification is shown in Figure 10.

Before the unbalance response experiment, the rotor has been adjusted to nearly balanced condition under the dynamic balancing machine to avoid the residual unbalance influence from the rotor itself. When the rotational frequency is greater than 300 Hz, the rotor displacement response amplitude is bigger under the unbalanced excitation. In view of the stability and safety of system, the rotational frequency in this paper is below 300 Hz. Figure 11 is the comparison charts of each finite element simulation amplitude and testing unbalance response amplitudes.

As can be seen from Figure 11, when the rotational frequency is below 200 Hz, the finite element model of rotor bearing can be established based on the testing stiffness and damping in the rotor static suspension. The unbalance response amplitudes obtained by the simulation of rotor operation are basically consistent with the testing unbalance response amplitudes. This shows that the impact of speed on the radial AMBs parameters is very small, which means that the bearing parameters are mainly related to the frequency characteristics of the control system. That is, when the rotor speed is Ω, bearing parameters are basically consistent with the bearing parameters corresponding to the static suspension and the excitation frequency $\omega = \Omega$.

However, when the rotational frequency is above 200 Hz, there is large difference between the finite element simulation amplitudes and the testing amplitudes in 1# and 2#. And the finite element simulation amplitudes and the testing amplitudes in 3# and 4# also have certain difference. Parameters are not only related to the frequency characteristics of the control

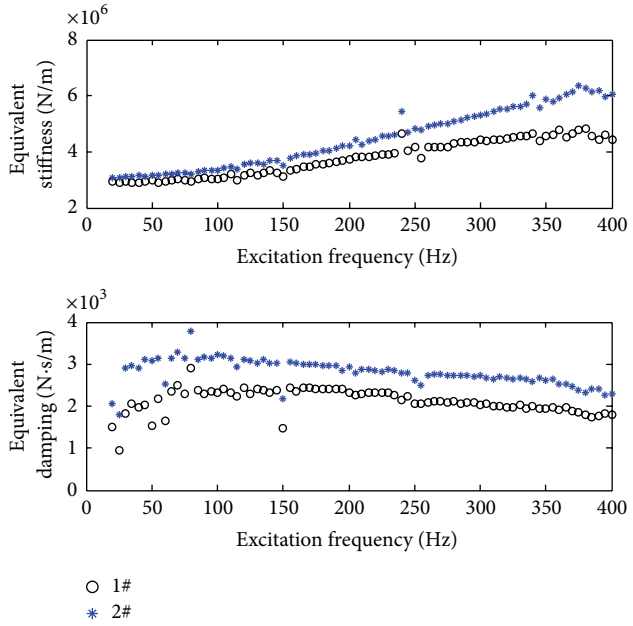

Figure 8: The stiffness and damping in 1#, 2#.

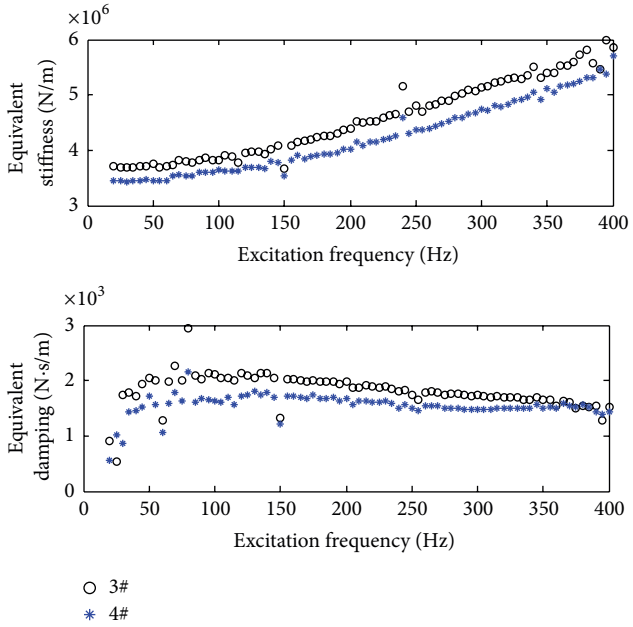

Figure 9: The stiffness and damping in 3#, 4#.

system but also related to the speed factor. This is mainly because the eddying effect in high speed influences the bearing characteristics of system, which leads to the difference of the amplitudes of two kinds of model. The difference between the finite element model and the actual rotor model and the difference between the unbalanced incentive of finite element model and the unbalanced mass of actual test are also the cause of the difference of the amplitudes of two kinds of model.

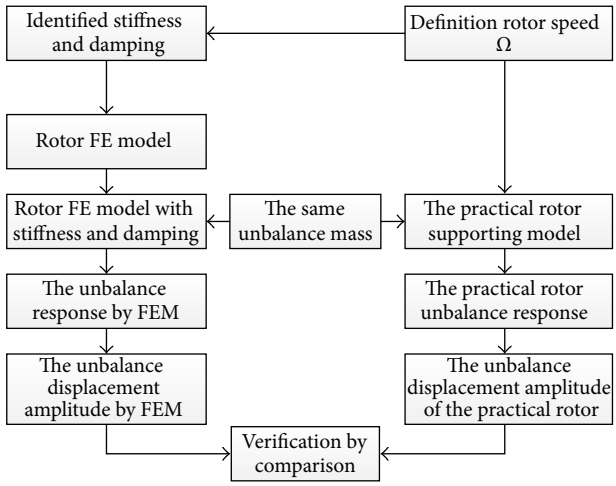

Figure 10: Testing flow chart.

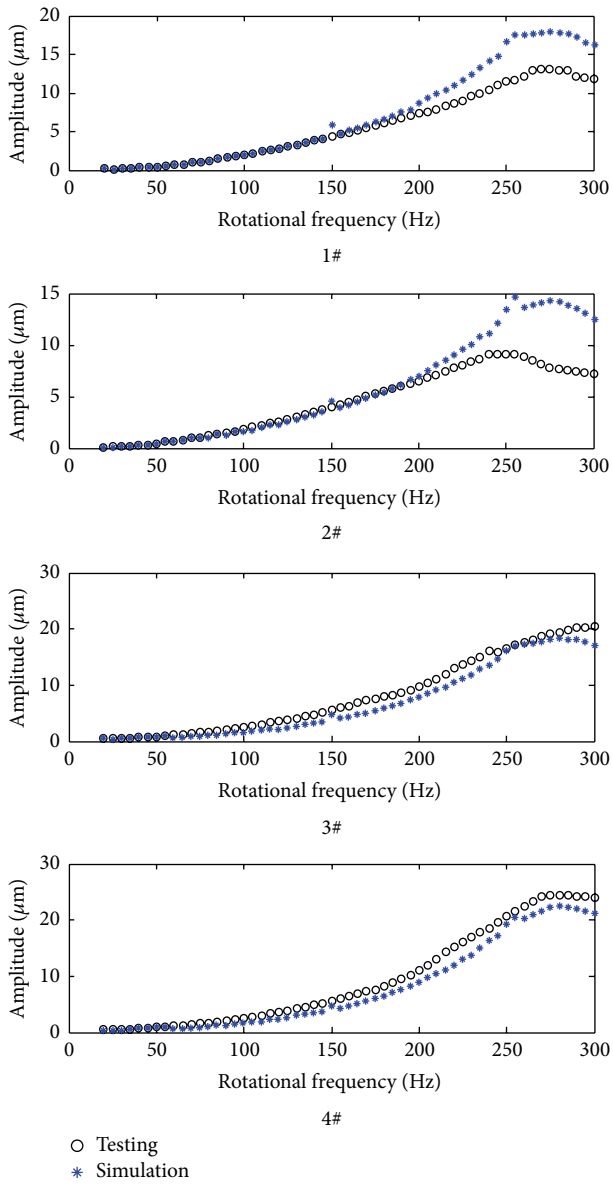

Figure 11: Simulation and measured rotor unbalance responses.

5. Conclusions

(1) This paper studies the relationship between the AMBs bearing parameters and the frequency characteristics of control system using the experimental method. By employing the magnetic bearings as a magnetic exciter, the AMBs stiffness and damping coefficients are obtained under the frequency domain, which is a simple and convenient method.

(2) This paper verifies the rationality of the testing AMBs parameters through the comparison of the finite element simulation amplitudes and the testing amplitudes using the unbalance excitation.

(3) The experimental results show that at low speed the bearing parameters are mainly determined by the controller characteristics. While at high speed, the bearing parameters are not only related to the control rule but also related to the speed. This may be due to the influence of eddying effect.

Conflict of Interests

The authors declare that there is no conflict of interests regarding the publication of this paper.

Acknowledgments

The authors gratefully acknowledge support of this research from National Natural Science Foundation of China (51205186), from the National Science Foundation for Postdoctoral Scientists of China (2012M511264), and from the Specialized Research Fund for the Doctoral Program of Higher Education of China (20123218120024).

References

[1] J. Zhou and Z.-X. Ni, "Identification method for stiffness and damping of magnetic bearings based on rotor unbalance responses," *Journal of Vibration and Shock*, vol. 32, no. 3, pp. 29–34, 2013.

[2] B. Zhang, Q. Guo, G. Chen, and Z. Xie, "Parameter identification of active magnetic bearing support based on finite element model updating using complex modal data," *Journal of Nanjing University of Aeronautics & Astronautics*, vol. 42, no. 6, pp. 748–752, 2010.

[3] O. C. De Santiago and L. San Andrés, "Field methods for identification of bearing support parameters—part I: identification from transient rotor dynamic response due to impacts," *Journal of Engineering for Gas Turbines and Power*, vol. 129, no. 1, pp. 205–212, 2007.

[4] O. C. De Santiago and L. San Andrés, "Field methods for identification of bearing support parameters. Part II. Identification from rotor dynamic response due to imbalances," *Journal of Engineering for Gas Turbines and Power*, vol. 129, no. 1, pp. 213–219, 2007.

[5] S. H. Bi, N. H. Li, and G. T. Zheng, "Field identification of the dynamic characteristic parameters of journal bearings and the unbalances of rotors," *Acta Aeronautica et Astronautica Sinica*, vol. 19, no. 3, pp. 378–382, 1998.

[6] S. G. Wang and Y. M. Xia, "Stiffness parameter extraction of rolling element bearings from random response," *Journal of Vibration Engineering*, vol. 17, no. 4, pp. 388–392, 2004.

[7] S. Q. Chen, X. W. Jiang, and X. Y. Wu, "Application of boundary element method to measuring dynamic stiffness and damping of bearing," *Journal of Naval University of Engineering*, vol. 20, no. 3, pp. 66–70, 2008.

[8] R. Tiwari, A. W. Lees, and M. I. Friswell, "Identification of speed-dependent bearing parameters," *Journal of Sound and Vibration*, vol. 254, no. 5, pp. 967–986, 2002.

[9] R. Tiwari, "Conditioning of regression matrices for simultaneous estimation of the residual unbalance and bearing dynamic parameters," *Mechanical Systems and Signal Processing*, vol. 19, no. 5, pp. 1082–1095, 2005.

[10] R. Tiwari and V. Chakravarthy, "Identification of the bearing and unbalance parameters from rundown data of rotors," in *IUTAM Symposium on Emerging Trends in Rotor Dynamics*, vol. 1011 of *IUTAM Bookseries*, pp. 479–489, Springer, Dordrecht, The Netherlands, 2011.

[11] X. Wang, "Analysis on stiffness and damping performaces of an active magnetic bearing system," *Chinese Journal of Applied Mechanics*, vol. 14, no. 3, pp. 95–100, 1997.

[12] L. Zhao, H. Cong, and H. B. Zhao, "Study on stiffness and damping characteristic of active magnetic bearing," *Journal of Tsinghua University (Science and Technology)*, vol. 39, no. 4, pp. 96–99, 1999.

[13] R. R. Humphris, R. D. Kelm, D. W. Lewis, and P. E. Allaire, "Effect of control algorithms on magnetic journal bearing properties," *Journal of Engineering for Gas Turbines and Power*, vol. 108, no. 4, pp. 624–632, 1986.

[14] R. D. Williams, F. J. Keith, and P. E. Allaire, "Digital control of active magnetic bearings," *IEEE Transactions on Industrial Electronics*, vol. 37, no. 1, pp. 19–27, 1990.

[15] T. M. Lim, D. Zhang, J. Yang et al., "Design and parameter estimation of hybrid magnetic bearings for blood pump applications," *Mechanical Systems and Signal Processing*, vol. 23, no. 7, pp. 2352–2382, 2009.

[16] N.-C. Tsai, H.-Y. Li, C.-C. Lin, C.-W. Chiang, and P.-L. Wang, "Identification of rod dynamics under influence of Active Magnetic Bearing," *Mechatronics*, vol. 21, no. 6, pp. 1013–1024, 2011.

[17] Y. Xu, J. Zhou, L. Di, C. Zhao, and Q. Guo, "Active magnetic bearing rotor model updating using resonance and MAC error," *Shock and Vibration*, vol. 2015, Article ID 263062, 9 pages, 2015.